Diffusive motion of C_{60} on a graphene sheet

M. Neek-Amal,[1,*] N. Abedpour,[2,3] S. N. Rasuli,[3,4] A. Naji,[3] and M. R. Ejtehadi[2]
[1]*Department of Physics, Shahid Rajaee Teacher Training University, Lavizan, P.O. Box 16785-136, Tehran, Iran*
[2]*Department of Physics, Sharif University of Technology, P.O. Box 11155-9161, Tehran, Iran*
[3]*School of Physics, Institute for Research in Fundamental Sciences (IPM), P.O. Box 19395-5531, Tehran, Iran*
[4]*Department of Physics, University of Guilan, P.O. Box 41335-1914, Rasht, Iran*
(Received 22 October 2009; revised manuscript received 11 August 2010; published 22 November 2010)

The motion of a C_{60} molecule over a graphene sheet at finite temperature is investigated both theoretically and computationally. We show that a graphene sheet generates a van der Waals laterally periodic potential, which directly influences the motion of external objects in its proximity. The translational motion of a C_{60} molecule near a graphene sheet is found to be diffusive in the lateral directions, while in the perpendicular direction, the motion may be described as diffusion in an effective harmonic potential which is determined from the distribution function of the position of the C_{60} molecule. We also examine the rotational diffusion of C_{60} and show that its motion over the graphene sheet is not a rolling motion.

DOI: 10.1103/PhysRevE.82.051605 PACS number(s): 68.43.−h, 65.60.+a

I. INTRODUCTION

Various properties of graphene as a new two-dimensional material have been studied both experimentally and theoretically [1,2]. Recent experimental research based on transmission electron microscopy (TEM) visualization studies the images and dynamics of light atoms deposited on a single-layer graphene sheet [3]. In general, the diffusion process and crystallization of atoms and light molecules on various surfaces have been subject of research for many years. The example of diffusive motion of inclusions over a rough membrane is an example which has recently received a lot of attention [4–6]. For instance, one may look at the solidification of C_{60} molecules (over various substrates and particularly) on graphene which has been a subject of recent interest. Some groups have experimentally studied the van der Waals epitaxy of a solid C_{60} over graphene sheet [7]. Also various dynamical properties of the spinning motion of C_{60} on the Au(111) surface have been studied by Teobaldi and Zerbetto by means of molecular-dynamics (MD) simulations [8]. A careful analytical study of the interaction and adsorption of C_{60} on various substrates such as graphite has been done by Gravil *et al.* [9]. They deduced that at room temperature C_{60} molecules are expected to be mobile on the graphite surface. The intercalation of C_{60} into graphite using synthesis and characterization of graphite is also possible [10,11]. The TEM image shows that the interaction between C_{60} molecules and graphene is not a covalent-type bond (neither between C_{60} molecules themselves nor between C_{60} and a graphene layer) [11]. It is rather described by the long-range van der Waals attraction as well as other repulsive atomic interactions that arise at very short distances [8,9].

The theoretical study of the motion of molecular scale inclusion on various surfaces is applicable to understand the motion of nanoscale inclusions over nanoelectromechanical surfaces (e.g., graphene). These studies play an important role in designing graphene-based nanosensors. Two main approaches for investigating the diffusive motion of an external inclusion on a membranes surface can be introduced. The first one is based on the continuum description for the membrane structure and introduces an effective Hamiltonian which can be used to study curvature-coupled diffusion [5,4,6]. The elastic aspects of the membrane thus play a key role in this approach. The second approach is an atomistic one which considers the details of the membrane and inclusion structures, as well as atomic interactions on different levels of coarse graining [12,13].

The diffusive motion of particles may be modeled generally via a Langevin equation. Lacasta *et al.* modeled general two-dimensional solid surfaces using a two-dimensional potential both with a deterministic periodic potential and a random one [14]. Different values for dissipation parameters generate different trajectories for a pointlike particle over such potentials, which thus lead to different dynamical behaviors ranging from subdiffusive to superdiffusive motion [14].

The choice of van der Waals parameters of C_{60}-graphene interaction is an important issue for performing any molecular-dynamics simulations. The C_{60}-carbon nanotube interaction can be obtained both experimentally and theoretically [15]. Several van der Waals parameters for physical adsorption of C_{60} on graphite and other substrates were formulated using a continuum rigid body model for C_{60} and a continuum dielectric media for graphite by Girard *et al.* [16]. The charge transfer from graphene to the C_{60} molecule is an open question which may be tackled using modern density-functional theories. For alkali metals on the graphite there have been some calculations in order to estimate transferred charges [17].

In a previous study we showed that the alkali and transition metals distribute over graphene and bind to its surface via a Lennard-Jones (LJ) potential and construct atomic nanoclusters [18]. For metallic nanoclusters, no diffusive motion was found in low temperature. It is also found that potassium atoms, in low temperature, construct a particular phase on the graphene sheet as well as on the graphite [17]. There have been only a few numbers of studies on the inter-

*Corresponding author; neekamal@srttu.edu

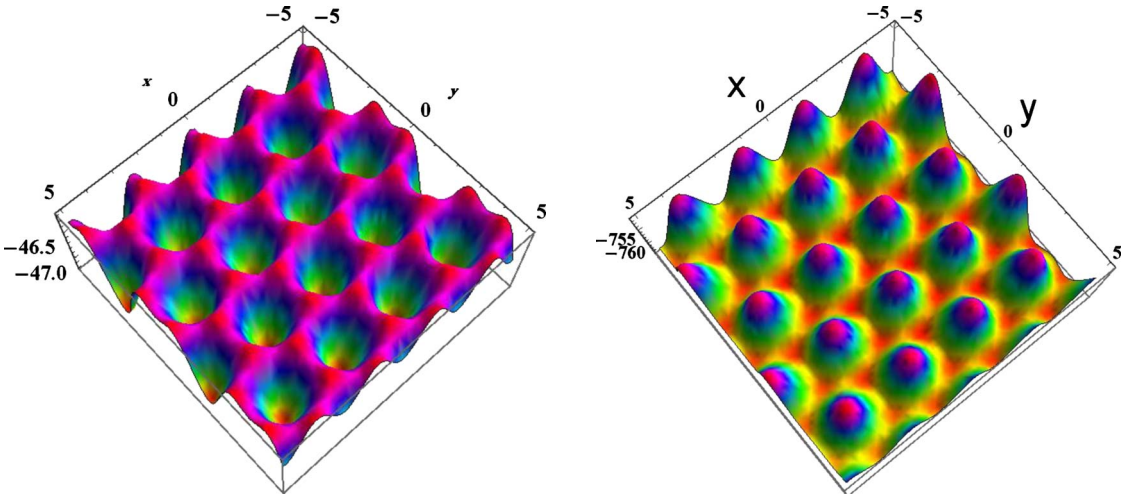

FIG. 1. (Color online) Left: periodic two-dimensional potential $\tilde{V}(x,y)$ created by the graphene sheet. Here, x and y refer to spatial position at the height z_0=3.5 Å above the graphene sheet. Right: periodic two-dimensional potential experienced by C_{60} molecules near a graphene sheet. In this case x and y are the center of mass coordinates of C_{60} measured from an origin on the sheet at the height z =6.5 Å. This is obtained by summing the potential experienced by all individual atoms comprising the C_{60} molecule.

action between graphene and inclusions that address the pattern of inclusion motion [4–6].

In this paper we study the dynamics of a single molecule, specifically chosen as the C_{60} molecule, on a graphene surface. We show that a graphene sheet creates a periodic van der Waals potential in its surrounding space, and that there are some simple criteria to determine when a molecule may diffuse through the potential wells generated by the graphene (as assisted by thermal fluctuations) or be likely to be trapped in the potential wells near the surface. We introduce a laterally averaged effective potential for the graphene sheet from the distribution function of C_{60} near the surface, and show that this potential may be approximated best by a harmonic potential in the direction normal to the sheet. We also introduce an effective friction coefficient for the diffusive motion of C_{60} over graphene. Finally, we show that the motion of C_{60} over graphene is not a rolling motion and also the variation of the perpendicular component of angular velocity of C_{60} is greater than its component parallel to the graphene sheet.

II. METHODS

We employ a classical MD algorithm to simulate the C_{60}-graphene system. The graphene is modeled as a square-like sheet of area 1883 nm^2 constructed with 72 000 carbon atoms. The temperature was kept constant (300 K) in our simulations by employing a Nosé-Hoover thermostat. For the covalent bounds between the nearest-neighbor atoms of the graphene sheet (and for chemically bonded atoms in C_{60} molecule) we have used Brenner's potential [19]. For the interaction between each atom of graphene with each of C_{60} atoms, we have used the LJ potential

$$U_{LJ} = 4\varepsilon\{(\sigma/r)^{12} - (\sigma/r)^{6}\},$$

with typical values σ=3.4 Å and ε=2.4 meV [20]. Both theory and experiments indicate that the interaction between C_{60} and a graphene layer is not a strong covalent-type bond [10,11]. Instead it is described by a much weaker van der Waals interaction that on the pairwise level is given by the LJ potential, which is thus expected to provide a reasonable first-step model for this system [8,9].

A graphene sheet was initially positioned, on average, at z=0 plane, and the centers of the C_{60} molecule were placed above it at z=7 Å. The temperature-dependent molecular-dynamics simulations run for up to 2 ns.

III. TWO-DIMENSIONAL POTENTIAL OF GRAPHENE SHEET

First we study the periodic two-dimensional LJ potential that a flat graphene sheet creates near its surface. This quantity gives some insight into how graphene influences molecules such as C_{60} moving at its proximity. Note that, in general, graphene is not a flat sheet at finite temperature and exhibits some corrugations. These "ripples" affect both electronic and mechanical properties of graphene [22,23]. Such corrugation effects are present in the simulations to be discussed later in this paper (see Fig. 6, inset). However, for the purpose of the following discussions, the graphene sheet may be locally approximated with a flat sheet, since the size of the C_{60} molecule is much smaller than the typical lateral size of the ripples in the sheet [21] and is bigger than the typical amplitude of the ripples at room temperature (Fig. 6, inset).

A flat graphene sheet comprises two triangular Bravais sublattices (i.e., A and B lattices), and the LJ potential due to this sheet [15] can be written as the sum of these two sublattice potentials:

$$E_T(x,y,z) = V_{A\text{-}lattice} + V_{B\text{-}lattice}, \quad (1)$$

where (x,y,z) is the position for center of mass of the molecule, having N atoms, above the sheet. We may write the appropriate expression for $V_{A\text{-}lattice}$ as

$$V_{A\text{-}lattice} = 4\sum_{m,n}\sum_{l=1}^{N}\sum_{k=1}^{2}\frac{(-1)^{k+1}\sigma^{12/k}}{[(x+x_l-n-m/2)^2+(y+y_l-\sqrt{3}m/2)^2+(z+z_l)^2]^{6/k}}, \tag{2}$$

and for $V_{B\text{-}lattice}$ as

$$V_{B\text{-}lattice} = 4\sum_{m,n}\sum_{l=1}^{N}\sum_{k=1}^{2}\frac{(-1)^{k+1}\sigma^{12/k}}{[(x+x_l+1/2-n-m/2)^2+(y+y_l-\sqrt{3}m/2-\sqrt{3}/6)^2+(z+z_l)^2]^{6/k}}. \tag{3}$$

Here, m and n are integer numbers which count lattice points for each sublattice. The coordinate of the lth macromolecule's atom (x_l, y_l, z_l) is measured from the molecule's center of mass. The sum over k also is responsible for varying of fraction's power between 12 and 6, and switching its sign. Because of the short-range behavior of the LJ potential, we observed that using the cutoff of $|m| \geq 10$ or $|n| \geq 10$ leads to quite accurate results with negligible cutoff errors in the total potential or force. For simplicity in Eqs. (2) and (3) all lengths were rescaled by $a_1 = \sqrt{3}a_0$, where $a_0 = 1.42$ Å and energies are in units of ε, with a_1 being the length of primitive vector of sublattices.

A. Potential energy between a single carbon atom and a graphene sheet

At a fixed height above the graphene sheet, $z = z_0$, the total potential in Eq. (1) reduces to a two-dimensional potential $\tilde{V}(x,y)$, which is periodic in x and y. Assume that we have fixed the height of a pointlike particle, such as a carbon atom, at a given value. Figure 1 (left panel) shows this periodic two-dimensional potential for $z_0 = 3.5$ Å. This potential provides some insights into the diffusive motion or trapping of a pointlike particle close to the graphene sheet [3]. The required potential can be obtained from Eqs. (2) and (3) with $N=1$ and putting x_l, y_l, and z_l equal to zero. Figure 2 shows the variation of potential energy in the y direction at $x=0$ for five different heights. To show that the variation of $\tilde{V}(x,y)$ in the z direction appears to be similar to the LJ potential, with a different functionality, we averaged the above potential in the Wigner-Seitz primitive cells on both sublattices and plot the result in the bottom panel of Fig. 3. As can be seen from the figure the potential minimum between graphene sheet and the single carbon atom is deeper than the simple case of two interacting carbon atoms via the LJ interaction. Furthermore, the minimum distance ($z_{min} \sim 3.4$ Å) is not $z = 2^{1/6}\sigma \sim 3.8$ Å as it is in the usual LJ (solid blue curve in Fig. 3). The minimum point of V_z gives the equilibrium distance of a carbon atom over the graphene flat sheet.

Note that the particle will equilibrate with the graphene sheet and obtains a mean kinetic energy on the order of $K_B T$ in its two-dimensional lateral motion. If $K_B T \simeq 25.7$ meV is smaller than the potential barriers heights, the particle may be trapped in one of the potential wells. Since $\tilde{V}(x,y)$ is a two-dimensional potential, the particle could take various paths from one well to neighboring wells. But for simplicity we may roughly take the difference between maximum and minimum values of $\tilde{V}(x,y)$ appearing in Wigner-Seitz primitive cells as a measure of the barrier strength compared to the thermal energy $K_B T$. The top panel in Fig. 3 shows the difference between maximum and minimum ΔV in units of $K_B T$ for various values of the particle height.

B. Potential energy between C_{60} molecule and graphene sheet

In the case of molecules such as C_{60} considered here, the total two-dimensional potential is periodic as well [see Fig. 1 (right panel)]. The interaction between this molecule and the graphene sheet has several functional forms depending on the orientation of the molecule over the sheet even at a fixed height of the molecule's center of mass above the sheet. Two particular orientations of C_{60} are more interesting than the others. These two refer to the cases when a pentagon or a hexagon of C_{60} atoms faces the flat graphene surface. Figure 1 (right panel) is related to a C_{60} molecule when one of the pentagons is near the surface and the plane of the pentagon is parallel to the graphene sheet. Since the radius of the C_{60} molecule is $R_{C_{60}} = 3.54$ Å, it can never get closer to the surface than this distance. Figure 4 shows the variation of potential energy along normal direction for five different

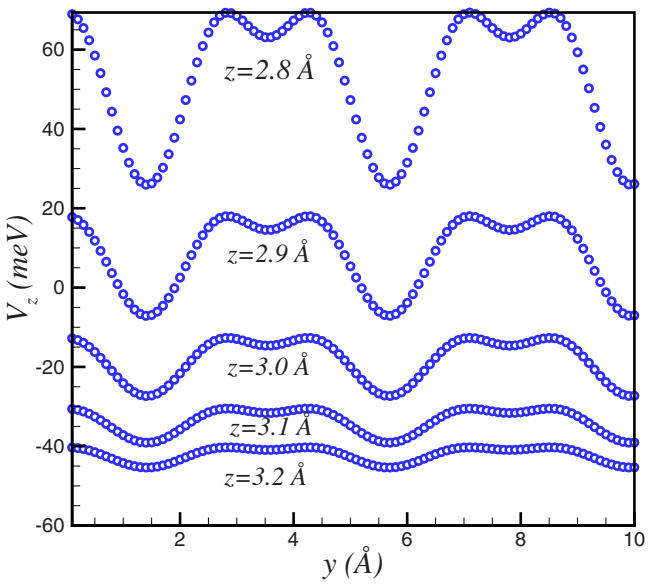

FIG. 2. (Color online) Periodic potential energy between flat graphene sheet and a single carbon atom at $x=0$ as a function of y for several height values.

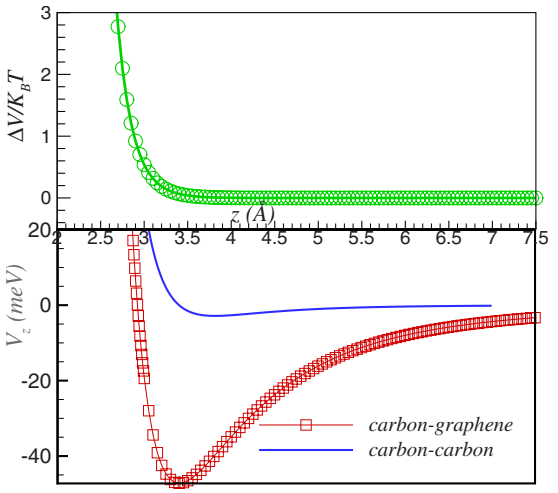

FIG. 3. (Color online) Top: difference between maximum and minimum of two-dimensional potential (averaged over Wigner-Seitz primitive cell of both A and B lattices) created by a flat graphene sheet (see Fig. 1) as a function of normal distance z as experienced by a single carbon atom. Bottom: total potential energy between a flat graphene sheet and a single carbon atom has been depicted. The solid (thick) blue curve is a simple LJ potential between two carbon atoms. In both panels, to eliminate the dependence on the x and y variables, we averaged over the first Brillouin zone of both A and B lattices. The data have small (10^{-5}) error bars, which are not shown.

heights of the center of mass of C_{60} molecule. Furthermore the variation of E_T along the z direction averaged over Wigner-Seitz primitive cells of A and B lattices is shown in the bottom panel of Fig. 5 (delta symbols). This gives the minimum height value for the center of mass of C_{60} molecule as $z_{min} \sim 6.5$ Å, which is obviously larger than the equilibrium distance obtained for a single carbon above the flat

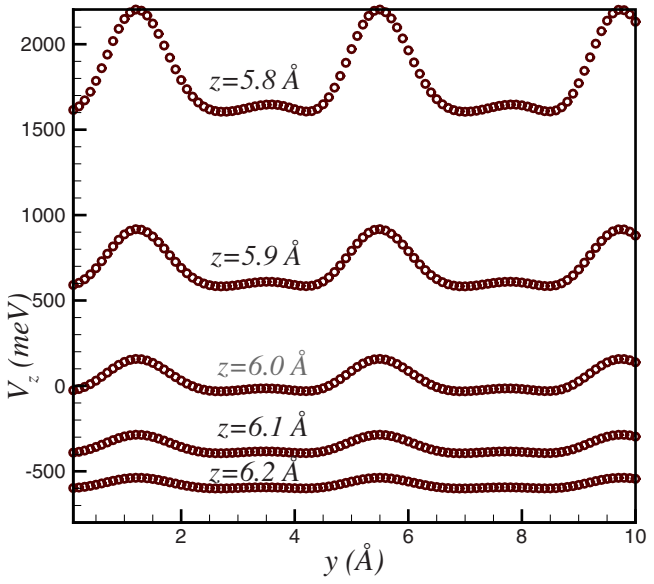

FIG. 4. (Color online) Periodic potential energy between C_{60} molecule and flat graphene sheet at $x=0$ as a function of y for several height values.

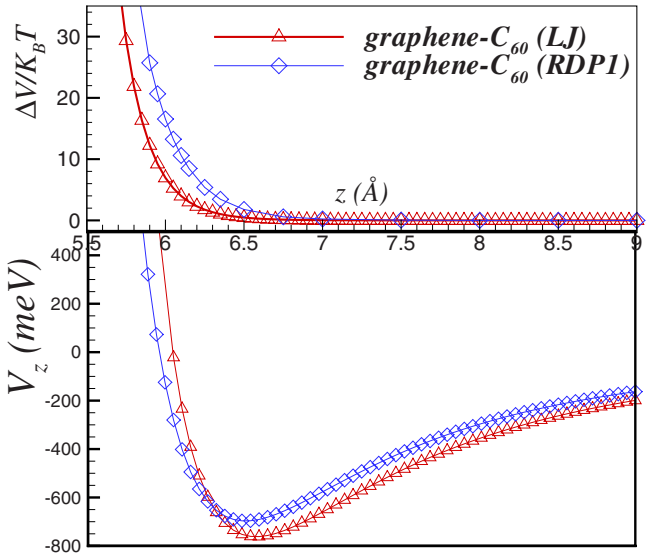

FIG. 5. (Color online) Top: difference between maximum and minimum of two-dimensional potential of a flat graphene sheet as experienced by a C_{60} molecule (see right panel of Fig. 1) as a function of the normal distance z. Bottom: total potential energy between a flat graphene sheet and a C_{60} molecule. In both panels, to eliminate the dependence of the x and y variables, we averaged over Wigner-Seitz primitive cells of both A and B lattices with the data have infinitesimal (10^{-5}) error bars, which were not shown. Here, open triangular symbols give LJ potential result and open diamond symbols give the RDP1 potential result.

sheet. Surprisingly this number is very close to that obtained by careful analytical study on adsorption of C_{60} molecule on the graphite [9]. The binding energy of C_{60} molecule and monolayer graphene can be estimated as $D=760$ meV, which is close to the experimental value for binding energy of C_{60} molecule and graphite bulk [15] and is close to the value predicted theoretically [9] (see Table I). It turns out that increasing the number of layers has only a small effect on the location of the minimum and the depth of the energy curve along the z axis [24].

Similar to the single carbon case we show the difference between maximum and minimum appearing in Wigner-Seitz primitive cells with respect to the thermal energy in the top panel of Fig. 5 (open triangles). The several orientations have no effect in the curves in Fig. 5. Furthermore, the height of saddle points in the potential profile in Fig. 1 (right panel)

TABLE I. Binding energy (D) and the equilibrium distance (z_{min}) of the center of mass of C_{60} over a graphene sheet from different models and experiments. The experimental value was reported for graphite.

Method	D (meV)	z_{min} (Å)
LJ	760	6.50
RDP1	696	6.43
Ref. [9]	955	6.56
Expt. [15]	850	

with respect to the thermal energy is around 0.2, which indicates that thermal energy is the dominant factor. Therefore, we expect that there should not be any trapping in the motion of C_{60} over graphene even at low temperatures and various orientations. In the next section we show that the motion coincides with a diffusive Brownian motion.

This foregoing observation about the size of C_{60} molecule and the ratio between thermal energy and the depth of the potential wells may be extended to other macromolecules and nanostructures such as buckyballs and carbon nanotubes. Almost all of these carbon allotropes have longitudinal and lateral dimensions larger than those of C_{60}. In a future work we will investigate dynamics of other carbon allotropes over this monolayer sheet at finite temperatures.

Before concluding this section it is worthwhile to discuss the prediction of other force fields for the energy variation and energy barriers for the motion of C_{60} over graphene. The combination of the results obtained from density-functional theory with experimental information on the exfoliation energy gives an improved registry-dependent potential (RDP1) for the interlayer interaction in graphitic structures [25,26]. Since the real π overlap between graphite layers is anisotropic, it cannot be described in a natural way by the single length scale of a LJ potential. The results of this potential for the corrugation against sliding for armchair and zigzag nanotubes over the graphene sheet overestimate corrugations with respect to those proposed from LJ potential [25]. Here, we repeat our calculations for the potential profile experienced by a C_{60} molecule close to a flat graphene sheet by using the RDP1 [25,26]. The results from using the RDP1 (open diamonds) are shown along with those obtained from the LJ potential (open triangles) in Fig. 5. As one can see from Table I, the depth D of the minimum of the RDP1 energy curve along the z axis (bottom panel) is about 18% smaller than the experimental value and is about 8% smaller than the corresponding LJ value. On the other hand, the RDP1 gives a slightly smaller value for the location of the minimum, z_{min}. The difference between the heights of maximum and minimum of the two-dimensional potential profile due to RDP1 is shown in the top panel of Fig. 5 (open diamonds) and is compared with those from the LJ potential (open triangles). The difference between the LJ and RDP1 models for C_{60} over graphene is not as high as those obtained in Ref. [25] for nanotubes over graphene and multiwall carbon nanotubes. In particular, near z_{min} and further away from the sheet, where the C_{60} molecule actually spans most of its (diffusion) time, the difference between the LJ and RDP1 models is negligible.

IV. TRANSLATIONAL DIFFUSION

In Fig. 6, the mean-square displacement $\langle R^2 \rangle$ of an ensemble of 30 C_{60} molecules moving near a graphene sheet at room temperature is plotted as a function of time for the projected two-dimensional motion onto the x-y plane, where $R^2=x^2+y^2$. The inset of the figure shows the x-y trajectory for a single C_{60} molecule. The total simulation time is 2.5 ns. The diffusion coefficient for the C_{60} molecule is obtained from this graph as $D=7.0\times10^{-8}$ $m^2\ s^{-1}$. Using Einstein's relation, we estimate an effective friction coefficient of $\xi = K_BT/D = 1.4\times10^7$ $m^{-2}\ s \times K_BT$ for C_{60} moving near a graphene sheet. At very short times the observed motion is not diffusive because we put all C_{60} at the center of the membrane with initial random velocities extracted from a Maxwell-Boltzmann distribution, and the graphene is not in thermal equilibrium with those molecules. Therefore, at very short time of about 5 ps, the C_{60} molecules attempt to find the minimum energy trajectories, yet their total displacement is not significant.

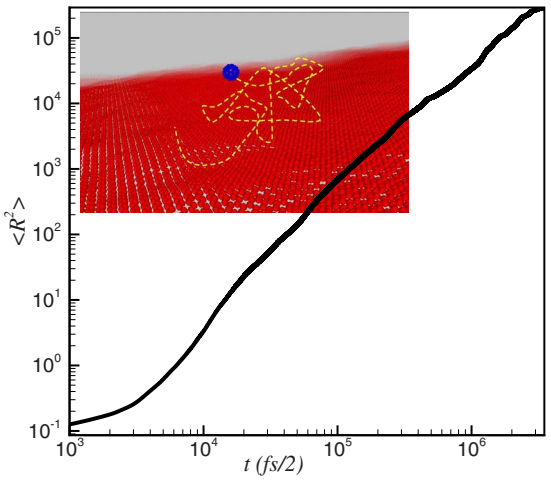

FIG. 6. (Color online) Mean-square displacement $\langle R^2 \rangle$ versus time for the lateral motion of an ensemble of 30 C_{60} molecules moving near a graphene sheet at room temperature. Inset shows a typical x-y trajectory of a single C_{60} on the graphene sheet.

V. EFFECTIVE POTENTIAL FOR VIBRATIONAL MOTION IN THE z direction

In our MD simulations the C_{60} molecule does not unbind from the graphene sheet. We may introduce an effective potential for the C_{60} motion in the z direction by calculating the distribution function $p(z)$ of the height of a C_{60} molecule above the sheet. By virtue of the Boltzmann factor, we may define the effective potential as $U/K_BT=-\log[p(z)]$, which embeds in itself both entropic and energetic factors related to the equilibrated motion of C_{60} near the graphene sheet. Results are represented in Fig. 7. It turns that the effective potential has a harmonic-type shape and $U/K_BT \cong \frac{1}{2}k(z-z_m)^2$ with the effective parameters k and z_0 obtained from a best fit as $k=1.255K_BT$ (N/Å) and $z_m=5.908$ Å. One thus expects that the C_{60} molecules effectively exhibit bounded vibrational motion in the normal direction to the graphene sheet. In lateral directions, as we discussed in the previous sections, the motion is diffusive. Here, the mean value for $\langle z \rangle = 5.975$ Å shows the equilibrium distance of center of mass of C_{60} molecule which already has been thermalized with the graphene sheet. This value of height depends on the temperature of the system. Note that this equilibrium distance is calculated for the rough graphene unlike the value reported in Sec. III. The distance from graphene sheet is thus found to be bigger than the distance of C_{60} from the first layer of gold

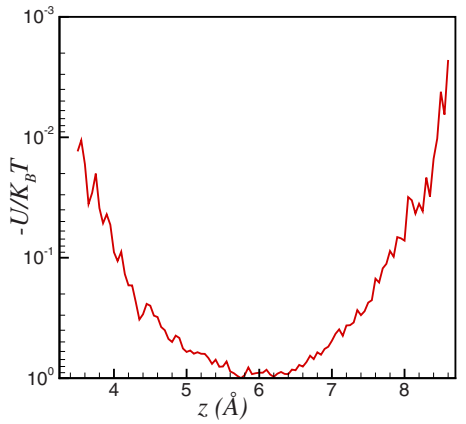

FIG. 7. (Color online) Effective potential of the interaction between a C_{60} molecule and a graphene sheet.

bulk [8], i.e., 5.4 Å. This is because the graphene sheet is a single atomic layer instead of a bulk material.

VI. ROTATIONAL DIFFUSION

Rotation matrix transforms the coordinates of a vector in body-fixed frame to the coordinates in the laboratory-fixed frame. We define the body-fixed frame as two perpendicular vectors, which are chosen as two lines connecting two pairs of opposite points on the C_{60} cage and the cross vector of those two vectors. In order to be sure about the orthonormality of those vectors the Gram-Schmidt orthonormalization processes was applied in each time step of simulation.

The quaternion representation of rotation matrix is a useful method for numerical simulations since it is more numerically stable [27]. The angular velocities of C_{60} in the body-fixed frame can be written in terms of quaternions and their time derivatives. Applying the inverse of the rotation matrix on the angular velocity of C_{60} in the body-fixed frame yields the angular velocities of C_{60} in the laboratory-fixed frame, $\vec{\omega}$.

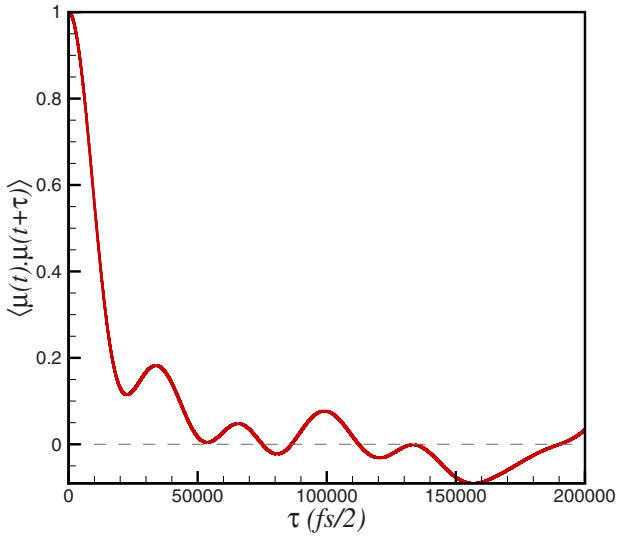

FIG. 8. (Color online) Rotational correlation: the correlation length of μ is about 75 000 steps (37.5 ps).

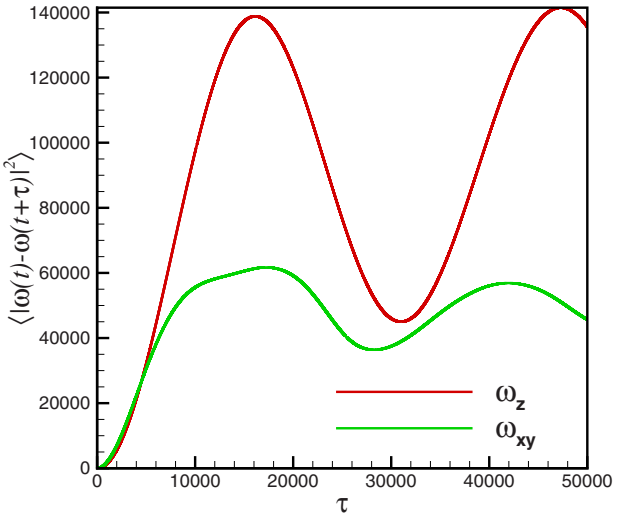

FIG. 9. (Color online) Increments of ω_z (top) and ω_{xy} (bottom) versus time step.

To show that the motion of C_{60} on the graphene is not a rolling motion, we have calculated the cross correlation of the unit vector of angular velocity, $\hat{\omega}$, and the unit vector of velocity, $\hat{v}$, i.e., $\langle \hat{\omega} \cdot \hat{v} \rangle = 3.0 \times 10^{-2} \pm 0.01$ and $\langle |\hat{\omega} \cdot \hat{v}| \rangle = 0.47 \pm 0.01$. Note that the first average is almost zero, but it cannot be confirmed that these two vectors are uncorrelated because this average becomes zero for two perpendicular vectors as well. On the other hand, the nonzero second average shows that they are not perpendicular. Therefore, these two averages together make sure that these two vectors are uncorrelated. The independence of the direction of velocity from the angular velocity ensures that the motion of C_{60} over graphene sheet is not a rolling motion.

Defining a fixed vector in C_{60}, μ, helps us to investigate the diffusive nature of C_{60} motion. It can be understood from the time autocorrelation of μ where the correlation time is 37.5 ps (see Fig. 8). It is obvious that the correlation length of μ is about 75 000 steps, and it means that after this time the orientation of C_{60} becomes completely different. The angular velocity in different directions has different behaviors. Figure 9 shows the increments of ω_z and ω_{xy}. Obviously the fluctuations of ω_z are bigger than those of ω_{xy}. This is due to the structure of C_{60} which is not a continuous ball. It is a discrete spherical object. As we mentioned in the previous section the pairwise interaction of C_{60} with the graphene atoms depends on the several orientations of C_{60}. For example, when a hexagon of C_{60} is parallel to another hexagon in the graphene plane, C_{60} would be more stable than the other possible orientations. These restrictions do not affect the rotation around the z axis, so the rotation around the z axis is easier than around x-y direction.

VII. CONCLUSION

We studied the motion of C_{60} molecules over a graphene sheet. Both flat approximations for monolayer graphene sheet and monolayer graphene at a finite temperature have

been studied using atomistic simulations. The depth of the potential wells generated by a graphene sheet in its proximity decreases as the height of an external object increases above the sheet. The binding energy of C_{60} over a graphene sheet was found as 760 meV close to the experimental value for binding energy of C_{60} and graphite [15]. The motion of C_{60} in the perpendicular direction was found to be a vibrational motion similar to a simple harmonic oscillator, while the motion in lateral directions is found to be a diffusive nonrolling motion.

[1] K. S. Novoselov, A. K. Geim, S. V. Morozov, D. Jiang, Y. Zhang, S. V. Dubonos, I. V. Grigorieva, and A. A. Firsov, Science **306**, 666 (2004).

[2] A. K. Geim and K. S. Novoselov, Nature Mater. **6**, 183 (2007); A. K. Geim and A. H. MacDonald, Phys. Today **60**, 35 (2007); A. H. Castro Neto, F. Guinea, N. M. R. Peres, K. S. Novoselov, and A. K. Geim, Rev. Mod. Phys. **81**, 109 (2009).

[3] J. C. Meyer, C. O. Girit, M. F. Crommie, and A. Zettl, Nature **454**, 319 (2008).

[4] E. Reister-Gottfried, S. M. Leitenberger, and U. Seifert, Phys. Rev. E **75**, 011908 (2007).

[5] E. Reister and U. Seifert, EPL **71**, 859 (2005).

[6] A. Naji and F. L. H. Brown, J. Chem. Phys. **126**, 235103 (2007); A. Naji, P. J. Atzberger, and F. L. H. Brown, Phys. Rev. Lett. **102**, 138102 (2009).

[7] A. Hashimoto, K. Lwao, S. Tanaka, and A. Yamamoto, Diamond Relat. Mater. **17**, 1622 (2008).

[8] G. Teobaldi and F. Zerbetto, Small **3**, 1694 (2007).

[9] P. A. Gravil, M. Devel, Ph. Lambin, X. Bouju, Ch. Girard, and A. A. Lucas, Phys. Rev. B **53**, 1622 (1996).

[10] A. Kuc, L. Zhechkov, S. Patchkovskii, G. Seifert, and T. Heine, Nano Lett. **7**, 1 (2007).

[11] V. Gupta, P. Scharff, K. Risch, H. Romanus, and R. Muller, Solid State Commun. **131**, 153 (2004).

[12] K. S. Kim, J. C. Neu, and G. F. Oster, EPL **48**, 99 (1999); Biophys. J. **75**, 2274 (1998).

[13] O. Farago, J. Chem. Phys. **119**, 596 (2003).

[14] A. M. Lacasta, J. M. Sancho, A. H. Romero, I. M. Sokolov, and K. Lindenberg, Phys. Rev. E **70**, 051104 (2004).

[15] H. Ulbricht, G. Moos, and T. Hertel, Phys. Rev. Lett. **90**, 095501 (2003).

[16] Ch. Girard, Ph. Lambin, A. Dereux, and A. A. Lucas, Phys. Rev. B **49**, 11425 (1994).

[17] M. Caragiu and S. Finberg, J. Phys.: Condens. Matter **17**, R995 (2005), and references therein.

[18] M. Neek-Amal, R. Asgari, and M. R. Rahimi Tabar, Nanotechnology **20**, 135602 (2009).

[19] D. W. Brenner, Phys. Rev. B **42**, 9458 (1990).

[20] H. Rafii-Tabar, Phys. Rep. **390**, 235 (2004).

[21] N. Abedpour, M. Neek-Amal, R. Asgari, F. Shahbazi, N. Nafari, and M. R. Tabar, Phys. Rev. B **76**, 195407 (2007).

[22] W. Bao, F. Miao, Z. Chen, H. Zhang, W. Jang, C. Dames, and C. N. Lau, Nat. Nanotechnol. **4**, 562 (2009).

[23] M. Neek-Amal and F. M. Peeters, Phys. Rev. B **82**, 085432 (2010); Appl. Phys. Lett. **97**, 153118 (2010).

[24] M. Neek-Amal and A. Lajevardipour, Comput. Mater. Sci. **49**, 839 (2010).

[25] A. N. Kolmogorov and V. H. Crespi, Phys. Rev. B **71**, 235415 (2005).

[26] A. N. Kolmogorov and V. H. Crespi, Phys. Rev. Lett. **85**, 4727 (2000).

[27] D. C. Rapaport, *The Art of Molecular Dynamics Simulation* (Cambridge University Press, Cambridge, England, 2004).